Influence of Semi-Solid Compression Conditions on the Refinement of Si Particles in Hypereutectic Al–25mass% Si Alloy

Yasuyoshi Fukui, Daisaku Nara, Kazuyo Fushimi, Mitsuhiro Nakao, and Noriyoshi Kumazawa
Graduate School of Science and Engineering, Kagoshima University
Kagoshima, Japan
nara@eng.kagoshima-u.ac.jp

Abstract—The possibility of Si particle refinement in hypereutectic Al–25 mass% Si alloy was examined through uniaxial compression tests using cylindrical specimens at a temperature just over the eutectic melting point. The test conditions comprised a combination of temperatures 853 K (580 °C) and 863 K (590 °C), compression rates 5, 25, and 125 mm/min, and compression strokes 5, 10, and 12 mm. The compressed specimens, unlike the drop forged specimens, exhibited barrel shapes because of the relatively low compression rate. The deformation resistance at 853 K (580 °C) was two times greater than that at 863 K (590 °C), and the dominant factor governing the viscoplastic flow appeared to be the plastic flow. In this case, finer Si particles were obtained under test conditions of the lower test temperature, the highest compression rate, and the longest compression stroke. The variation of Si particle sizes exhibited a distinct dependence on the shear rate at each test temperature. No single parameter such as applied strain, strain rate, power, and power rate was the predominant factor governing Si particle refinement; instead, these factors apparently interact with one another. In consideration of the physicochemical reaction, the effects of the shear rate and test temperature on Si particle size were summarized by the empirical power-law equation. This relation indicates that high shear rate operation at a temperature just above the melting point of eutectic Al–Si alloy must be the optimum conditions for refining the Si particles.

Keywords— *viscoplastic deformation; hypereutectic; semi-solid forming; refinement of particle*

I. INTRODUCTION

The binary eutectic Al−Si alloy, whose chemical composition is 11.6 mass% Si and whose melting point is 850 K (577 °C), is well known to exhibit superior properties such as good castability, high corrosion resistance, good thermal conductivity, and low density. In addition, the hypereutectic Al−Si alloys containing 15−25 mass% Si exhibit excellent wear resistance and low thermal-expansion coefficients [1-4]. When the hypereutectic Al–Si alloy solidifies, the Si phase forms and grows in angular primary particles; the alloy then usually contains coarse, angular primary Si particles in a eutectic phase. The presence of this coarse and brittle Si phase prevents to get rid of a difficulty to achieve optimum mechanical properties. Thus, both the attainment of good ductility and an improvement of poor machinability are required to enable the utilization of the superior properties of hypereutectic Al−Si alloy. These shortcomings must be overcome by refining the Si particles and achieving a more uniform distribution. The primary obstacle to using hypereutectic Al−Si alloy in practical application is the difficulty associated with obtaining fine Si particles.

In a series of studies concerning with the Al base materials, we focused on functionally graded materials (FGMs) and developed a method for preparing them via our proposed centrifugal method [5-8]. The cooling rate in this method is so slow that unworkable combined materials, *e.g.*, intermetallics of Al_3Ni [5] and Al_3Fe [8], become coarse, and the presence of a coarse and brittle intermetallic phase complicates secondary processes such as plastic forming. We addressed this problem and examined near-net shape forming using a semi-solid material to overcome it. We observed that the coarse Al_3Ni intermetallics in Al−Al_3Ni FGM were refined when the FGM was worked at a temperature just over its melting point [5,8]. The similar refinement of coarse Si particles was observed in an Al−Si FGM specimen fabricated using hypereutectic Al−25 mass% Si alloy [9]. We therefore examined the refinement process in greater detail. Our near-net shape forming method differs from the well known thixoforming [10-13] in that our method does not involve stirring the semi-solid material; furthermore, our method has a distinctive characteristic in that coarse particles are refined by shear, abrasive, and crushing action during deformation.

The aim of the present work was to investigate the applicability of our semi-solid compression process for refining coarse Si particles in a hypereutectic Al−25 mass% Si alloy. Semi-solid cylindrical specimens were compressed under constant crosshead speeds as a processing experiment for producing a fine particulate Si phase. The effects of the test temperature, compression rate, and compression stroke on Si particle refinement were examined to

enable utilization of the superior nature of the hypereutectic Al–Si alloy. In the technical part of this investigation, we discuss the parameters related to the refinement of coarse Si particles using an empirical power-law equation based on the physicochemical effect.

II. EXPERIMENTAL PROCEDURES

The material used in this study was commercial-purity hypereutectic Al−25 mass% Si alloy; its chemical composition was 24.7 mass% Si, 0.14 mass% Fe, balance Al. Cylindrical specimens with a diameter D_o = 15 mm and a height h_o = 15 mm were cut using an electro-discharge machine from ingots. Semi-solid compression tests were performed using a 100 kN screw-driven universal high-temperature tension-compression machine (SHIMADZU AG-100kNX^{TM}) to examine the effects of the test temperature, compression rate, and compression stroke on the size of Si particles distributed in a eutectic matrix. The die and specimen set for the compression tests were heated in an electric furnace for 30 min and then compressed at an index temperature. The temperature was monitored using the output of a thermocouple inserted into the bottom of the container; the error was estimated to be ±2 K.

According to the Al–Si binary phase equilibrium diagram (Figure 1) [14], the test temperatures were selected as 853 K (580 °C) and 863 K (590 °C), which are higher than the solidus temperature of the eutectic (850 K, 577 °C); these temperatures were selected on the basis of our preliminary experiments [15]. Compression rates v of 5, 25, and 125 mm/min and compression strokes Δh of 5, 10, and 12 mm were also selected with consideration of the capabilities of the test machine. Thus, the experiments comprised 18 combinations: three different compression rates, three different compression strokes, and two different temperatures. The microstructural features of the specimens, including their morphology and the sizes of Si particles, were observed using a conventional optical microscope. The effects on the Si particle size were evaluated on the basis of the equivalent strain, mean strain rate, and shear rate. The power and power rate, which was calculated from the plot of measured load vs. displacement, were also used as an evaluation parameters.

III. RESULTS AND DISCUSSIONS

A. Features of Compressed Specimens

Semi-solid cylindrical specimens were compressed under predetermined conditions. Typical variations of deformed profiles under test conditions of T = 853 K (580 °C) and v = 125 mm/min are shown in Figure 2. The test temperature was just over the eutectic melting point of T_m = 850 K (577 °C). Figures 2 (a)–(d) show the profiles before compression and those after compression strokes of Δh = 5, 10, and 12 mm, respectively. The deformed specimens exhibited a barrel shape similar to that observed for ductile materials under some frictional restriction in uniaxial compression tests [16]. Moreover, vertical cracks were observed in Figures 2 (c) and (d); these cracks differed substantially from those observed in the drop forge tests (Figure 3) [15]. In Figure 3, the eutectic alloy melt is shown to have seeped through the solid material and then solidified as droplets because of the semi-solid condition of the sample. The tendencies of the barreling features at T = 863 K (590 °C) were similar to those observed in the case of T = 853 K (580 °C).

One explanation for the different features observed in Figures 2 and 3 appears to be the reverse tendency for slower strain rates to induce lower plastic flow resistance [17] and greater viscous flow resistance [18]. The major difference between the compression experiments and the drop forge experiments is the duration of compression, which is more than 10^3 times longer in compression experiments. Because of the slow compression rate, we inferred that the liquid material in the specimen, rather than moving
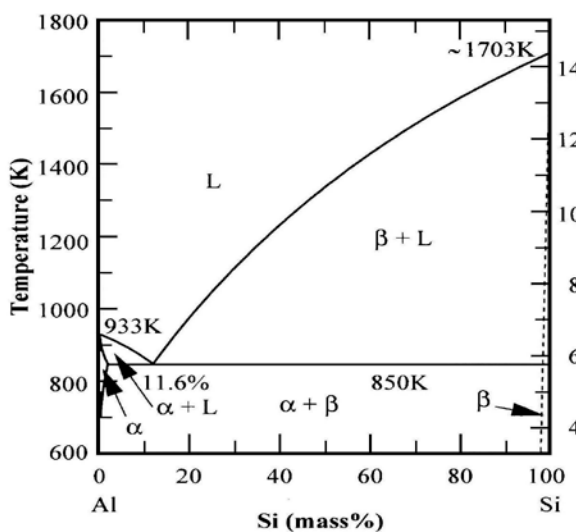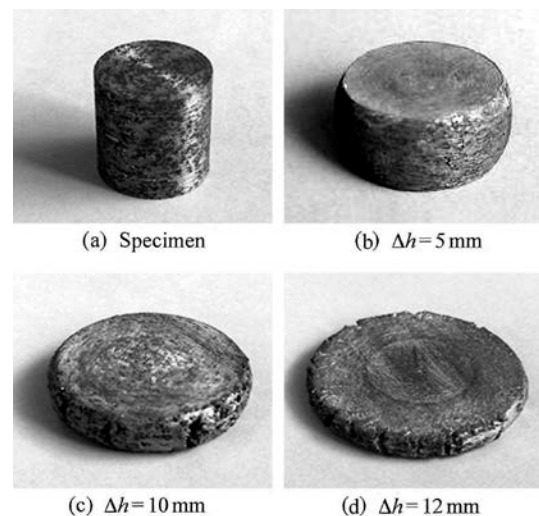

Fig. 1 *Al–Si binary alloy phase diagram.*

Fig. 2 *Typical variation in shape of compressed specimens deformed different compression stroke.*
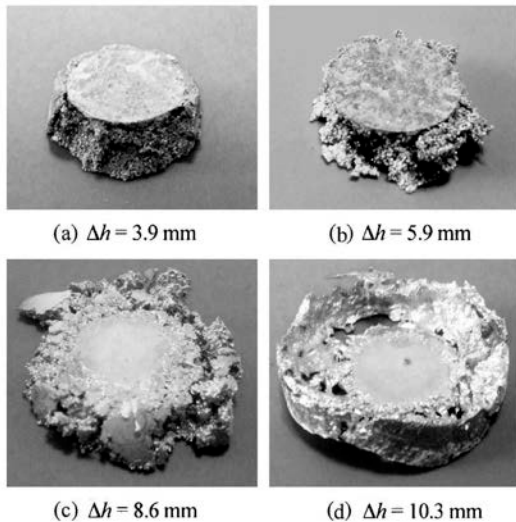
Fig. 3   *Typical variation in shape of drop forge specimens deformed different compression stroke.*

individually, moved together with the solid material under the experimental conditions, leading to the different features observed between Figures 2 and 3. We considered that the viscoplastic flow in the present mixture of solids and liquids must be controlled by the plastic flow and that the very slow compression rate, which led to relatively lower plastic flow resistance and greater viscous flow resistance, constrained the movement of the liquid component of the semi-solid specimen.

A microstructural study was conducting using an optical microscope to observe the morphology and size of the Si particles. Typical micrographs obtained from specimens that correspond to Figure 2 under test conditions of T = 853 K (580 °C) and v = 125 mm/min are shown in Figure 4. Figures 4 (a)–(d) show the microstructures of the as-received samples and those after compression strokes of Δh = 5, 10, and 12 mm, respectively. The white regions are the α-Al rich phase, *i.e.*, the eutectic Al–Si phase, and dark particles are the primary β-Si phase. In the case of the as-
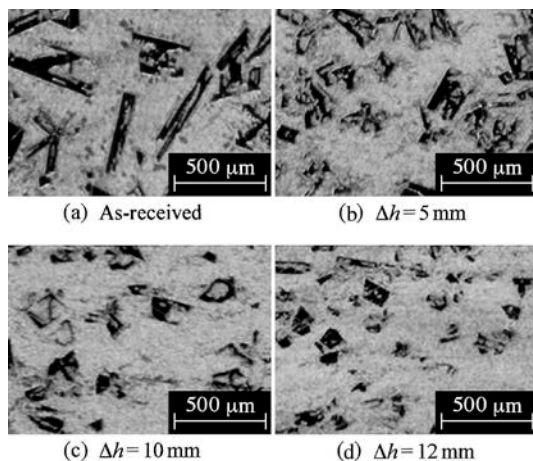

Fig. 4   *Typical variation in microstructure of compressed specimens of Al–25 mass% Si alloy.*

received sample, spindle-shape Si particles longer than 0.5 mm were occasionally observed among granular particles, as shown in Figure 4 (a); the average size of the Si particles was 0.270 mm. The averages shown in Figures 4 (b)–(d) were 0.155, 0.124, and 0.120 mm in the cases of Δh = 5, 10, and 12 mm, respectively. Coarse and angular primary Si particles became granular and refined with longer compression strokes. The overall ranges of Si grain sizes at 853 K (580 °C) and 863 K (590 °C) were 0.120–0.206 mm and 0.219–0.241 mm, respectively. The tendency of the Si particles to be refined with decreasing test temperature and increasing compression stroke and compression rate was confirmed.

B.   Effects of the Strain and Strain Rate on Si Particle Size

The effects of equivalent strain and mean strain rate on the refinement of Si particles were examined. The equivalent strain, $|\bar{\varepsilon}|$, and mean strain rate, $|\dot{\bar{\varepsilon}}|$, were calculated according to Equations (1) and (2), respectively:

$$|\bar{\varepsilon}| = -\log(1 - \Delta h / h_{\mathrm{o}}), \tag{1}$$

$$|\dot{\bar{\varepsilon}}| = |\bar{\varepsilon}| / t, \tag{2}$$

where h_{o} is the height of the specimen before the experiment and t is the duration of the compression stroke Δh. In Figure 2 (b)–(d), the equivalent strain and mean strain rate for compression strokes of Δh = 5, 10, and 12 mm in the case of v = 125 mm/min were calculated using Equations (1) and (2), respectively. The results were $|\bar{\varepsilon}|$ = 0.405 and $|\dot{\bar{\varepsilon}}|$ = 0.169 s^{-1}, $|\bar{\varepsilon}|$ = 1.10 and $|\dot{\bar{\varepsilon}}|$ = 0.229 s^{-1}, and $|\bar{\varepsilon}|$ = 1.61 and $|\dot{\bar{\varepsilon}}|$ = 0.279 s^{-1} for Figures 2 (b)–(d), respectively. The overall ranges of the equivalent strain and the strain rate were 0.405–1.61 and 0.00676–0.279 s^{-1}, respectively, independent of the test temperature.

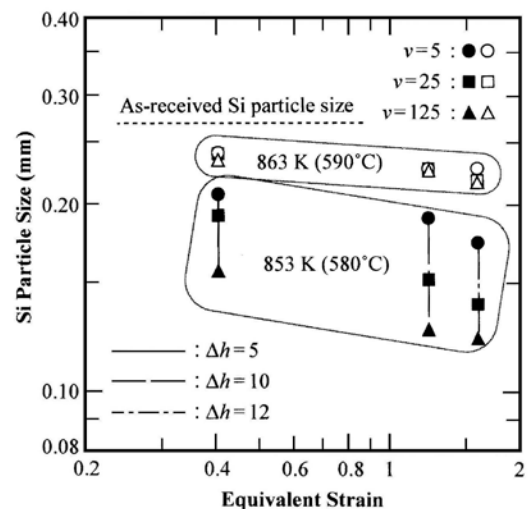Figures 5 and 6 show the variation of Si particle size as a function of the equivalent strain and the

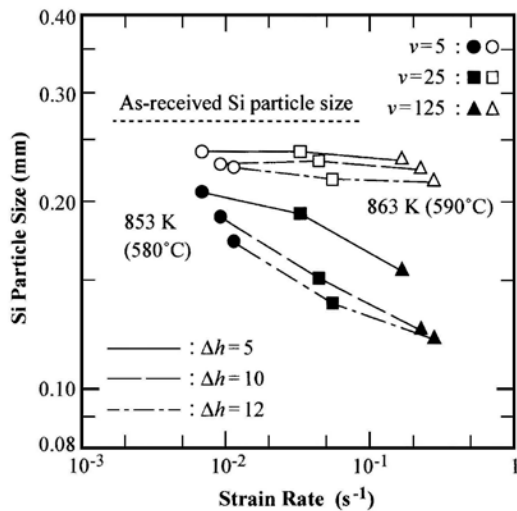Fig. 5   *Relationship between equivalent strain and Si particle size.*

Fig. 6   *Relationship between mean strain rate and Si particle size.*

Fig. 7   *Relationship between displacement and compressive load.*

mean strain rate, respectively, on a double-logarithmic chart. In Figures 5 and 6, the filled and open marks indicate the results obtained at T = 853 K (580 °C) and 863 K (590 °C), respectively; the circle, square, and triangle marks indicate the results obtained at v = 5, 25, and 125 mm/min, respectively; and solid, dotted, and single-dotted lines correspond to the results obtained at Δh = 5, 10, and 12 mm, respectively. The results for finest Si particles are plotted in the lower right-hand corner of Figures 5 and 6; these results were obtained under the conditions of T = 853 K (580 °C), Δh = 12 mm, and v = 125 mm/min. The corresponding micrograph is shown in Figure 4 (d). The Si particles tend to be more refined with increasing equivalent strain and the strain rate. Moreover, Si particles examined after the short compression stroke in the case of the faster compression rate at 853 K (580 °C) were also more refined. However, quantitative evaluation of the effect of the equivalent strain and the strain rate on the refinement of Si particles was difficult as evidence in Figures 5 and 6.

C.   Effects of the Power and the Power Rate on Si Particle Size

The variations of load as a function of displacement are summarized in Figure 7, which shows the load vs. displacement curves for T = 853 K (580 °C) and 863 K (590 °C); the solid, dotted, and single-dotted lines in the figure correspond to the results obtained at v = 5, 25, and 125 mm/min, respectively. An increase in the compression rate increased the compressive load, and the compressive load at 863 K (590 °C) was approximately half that at 853 K (580 °C). Moreover, the apparent yield stresses were calculated; those for T = 853 K (580 °C) were 8.5, 13.6, and 18.7 MPa in the cases of v = 5, 25, and 125 mm/min, respectively, and those for T = 863 K (590 °C) were 3.4, 6.2, and 10.2 MPa in the cases of v = 5, 25, and 125 mm/min, respectively. The higher test temperature and the slower compression rate
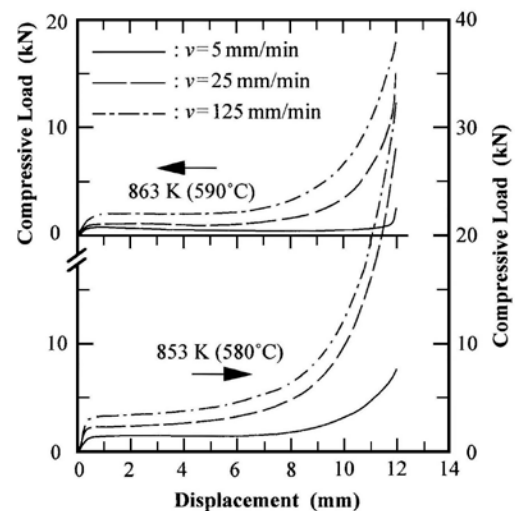
decreased the yield stress. This result is qualitatively similar to the tendency related to the effect of both working rate and working temperature on the deformation resistance under hot-working conditions. Thus, the dominant factor governing the viscoplastic flow is apparently the plastic flow, not the viscous flow. In Figure 7, the compression load was constant and/or gradually decreased up to $|\bar{\varepsilon}| \approx 0.9$ (approximately 6 mm compression stroke), even though the cross-sectional area increased.

To evaluate the effect of compressive load on the refinement of Si particles, both the power W and power rate w were calculated and examined. The power, which is related to the amount of consumed energy, is given by the following equation:

$$W = \int_0^t Pvdt, \tag{3}$$

where P is the compressive load, as shown in Figure 7, v is the compression rate, and t is the duration of load applied. The power rate, which represents the energy consumed per unit time, is the average value from zero to the pre-determined compression stroke Δh and is given as:

$$w = W/t, \tag{4}$$

The power and power rate were calculated using Equations (3) and (4), respectively; Figures 8 and 9 show the variation of Si particle size as a function of power and power rate, respectively, on double-logarithmic charts. In Figures 8 and 9, the filled and open marks indicate the results obtained at T = 853 K (580 °C) and 863 K (590 °C), respectively; the circle, square, and triangle marks indicated the results obtained at v = 5, 25, and 125 mm/min, respectively; and solid, dotted, and single-dotted lines correspond to the results obtained at Δh = 5, 10, and 12 mm, respectively. The power at 853 K (580 °C) and 863 K (590 °C) ranged from 7.00 to 90.5 J and from 2.88 to 48.6 J, respectively. The overall ranges of power rate at 853 K (580 °C) and 863 K (590 °C) were 0.117–15.7

W and 0.0479–8.43 W, respectively. Quantitative evaluation of the effect of the power and power rate on the refinement of Si particles was difficult. However, the tendency of Si particles to become more refined with increasing power and power rate in a manner similar to that shown in Figures 5 and 6 was confirmed. These results are consistent with the previous results that indicated finer dispersed Si particles were obtained at a temperature just over the eutectic temperature [7,8].
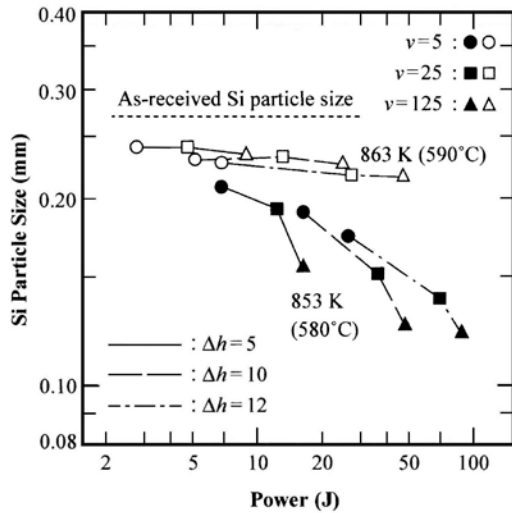

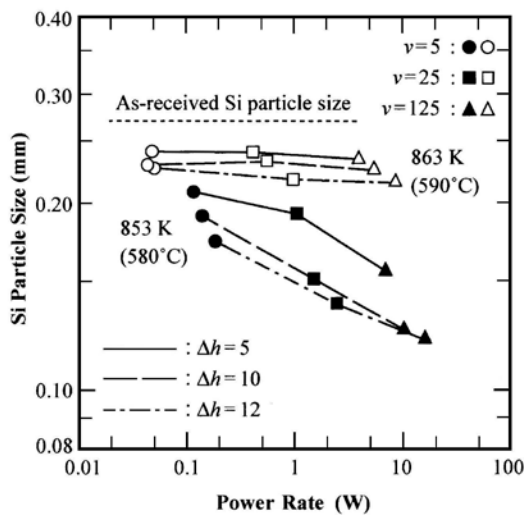Fig. 8 *Relationship between power and Si particle size.*

Fig. 9 *Relationship between power rate and Si particle size.*

D. Effect of the Shear Rate on Si Particle Size

We examined the effect of shear rate on the refinement of Si particles. The shear rate of cylindrical specimens under uniaxial compression were calculated using a cylindrical coordinate system (r, θ, z) with the origin of the z-axis (upward positive) being at the bottom center of the cylindrical specimen. The shear rate, $\dot{\gamma}$, under the assumption of a Newtonian fluid is given by the following equation [19]:

$$\dot{\gamma} = -\frac{6rz}{h^3}\frac{dh}{dt} \tag{5}$$

The volume-averaged shear rate, $\dot{\gamma}_{av}$, is then given as

$$\dot{\gamma}_{av} = \frac{2\pi}{V}\int_0^R \int_0^{h/2} \dot{\gamma}\, r\, dz\, dr = -\frac{R}{2h^2}\frac{dh}{dt} \tag{6}$$

where R is the outer radius of the specimen at time t and can be calculated from the constant-volume condition. Hereafter, the instantaneous volume averaged value given by Equation (6) is used as the shear rate, $\dot{\gamma}$.

Figure 10 shows on a double-logarithmic chart the variation of Si particle size as a function of shear rate calculated using Equation (6). In Figure 10, the filled and open marks indicate the results for $T = 853$ K (580 °C) and 863 K (590 °C), respectively; the circle, square, and triangle marks indicate the results for $v = 5$, 25, and 125 mm/min, respectively; and solid, dotted, and single-dotted lines correspond to the results for $\Delta h = 5$, 10, and 12 mm, respectively. The shear rates varied in the range from 3.83 ms^{-1} to 1.94 s^{-1} independent of the test temperature. These rates are more than 10^{-3} times slower than those observed for the drop forge tests [10] and these relatively slow shear rates are responsible for the morphological differences observed between Figures 2 and 3 as discussed in section 3.1.
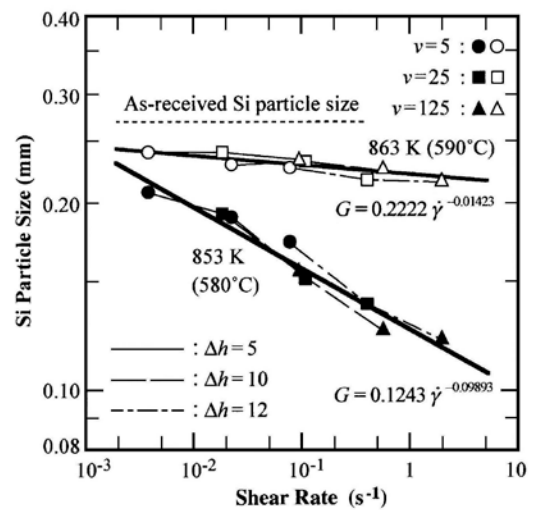

Fig. 10 *Relationship between shear rate and Si particle size.*

The Si particle size decreased with increasing of shear rate, as shown in Figure 10. The variation of Si particle sizes exhibited a distinct temperature dependence, and the effect of both the length of compression stroke and compression rate were concealed in the thick line. The relationship between shear rate, $\dot{\gamma}$ [s^{-1}], and Si particle size, G [mm], at each test temperature was established using the least-squares method; for $T = 853$ K (580 °C) and 863 K (590 °C), this relationship was established as

$$G = 0.1243\dot{\gamma}^{-0.09893}, \tag{7}$$

$$G = 0.2222\dot{\gamma}^{-0.01423}, \tag{8}$$

respectively. The correlation coefficients were −0.9743 and −0.9044 for T = 853 K (580 °C) and 863 K (590 °C), respectively, and a strong negative correlation was observed. The result was coincided with those, which indicated that the finer dispersed Si particles were obtained at a temperature just over the eutectic temperature [7,8].

E. Effect of the Test Temperature and Shear Rate on Si Particle Size

The Arrhenius and the Eyring models are well known as empirical formulas related to physicochemical effects in materials. The Arrhenius model represents the temperature dependence of reaction rates; the Eyling model, which is based on the Arrhenius model, expresses the relationship between reaction rate and energy, including stress variables other than the temperature. Both models are applicable to accelerated life testing and reliability determinations [20]. On the basis of such models, the refinement of Si particles is assumed to be decelerated under increasing temperature and to be accelerated under increasing shear rate. As such, the following empirical power-law model was examined:

$$G = A\Delta T^n \dot{\gamma}^{-B/\Delta T} = A(T - T_N)^n \dot{\gamma}^{-B/(T-T_N)} \tag{9}$$

where, A, B, and n are the positive constants and ΔT is the temperature difference between the reference temperature, T_N, and the test temperature, T. Equation (9) shows that the power-law index and constant are proportional to $(T - T_N)^{-1}$ and $(T - T_N)^n$, respectively.

Among the four constants in Equation (9), constants B and T_N were calculated first using the power-law indexes of −0.09893 in Equation (7) and −0.01423 in Equation (8) for T = 853 K (580 °C) and 863 K (590 °C), respectively. The results were B = 0.1662 and T_N = 851.32 K (578.32 °C). Then, A = 0.1063 and n = 0.3 were obtained using the power-law constants of 0.1243 in Equation (7) and 0.2222 in Equation (8) for T = 853 K (580 °C) and 863 K (590 °C), respectively. Thus, Equation (9) was represented as:

$$G = 0.1063(T - T_N)^{0.3}\dot{\gamma}^{-0.1662/(T-T_N)} \tag{10}$$

Given that the measured temperature error was ±2 K, the reference temperature was assumed to coincide with the eutectic melting point of $T_N = T_m$ = 850 K (577 °C); the temperature differences $\Delta T = (T - T_N)$ = 3 K and 13 K were subsequently obtained for T = 853 K (580 °C) and T = 863 K (590 °C), respectively.

In the case of $T_N = T_m$ = 850 K (577 °C), the remaining three constants A, B, and n were recalculated and obtained as A = 0.08, B = 0.24, and n = 0.4. Equation (9) was then rewritten as:
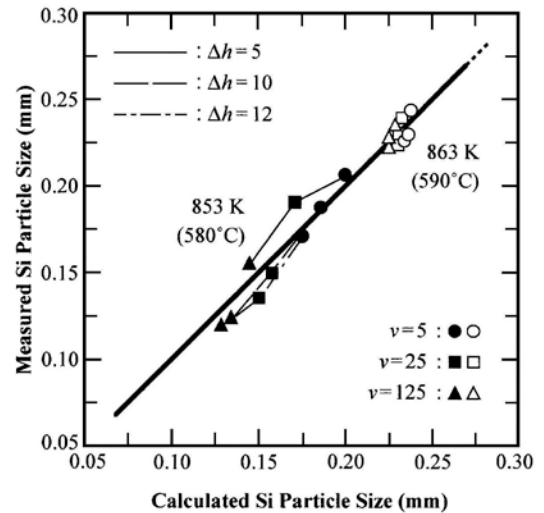

Fig. 11 *Comparison with the Si particle sizes of measured values and calculated values using Equation (11).*

$$G = 0.08(T - T_m)^{0.4}\dot{\gamma}^{-0.24/(T-T_m)}. \tag{11}$$

The Si particle sizes calculated using Equation (11) were compared with the measured Si particle sizes; the results are shown in Figure 11. In Figure 11, the points are plotted on a solid line showing the one-on-one relationship; they are consistent with the experimental results. The correlation coefficient is 0.960, which is slightly smaller than the coefficient of 0.978 obtained using Equation (10), and a strong positive correlation is confirmed. The formula based on the power-law rules of Equation (11) are consistent with the results obtained using Equation (10), which appears to be an appropriate approximation.

F. Conditions of Si Particle Refinement

The semi-solid forming enables the manufacture of products with both near-net shapes unachievable using plastic forming (forging) and superior mechanical properties unattainable using casting. Previous semi-solid experiments using a backward extruding [7-9] indicated that shear and abrasive forces arose from the viscoplastic flow of the eutectic semi-melt during a compression stroke and refined the coarse grains. One of the factors to be considered is the opposite effect, where a higher strain rate induces greater plastic flow resistance [17] and lower viscous flow resistance [18]. Additionally, both the plastic flow and viscous flow resistances are commonly acknowledged to decrease in tandem with the increase in working temperature. The necessary factor governing the viscoplastic flow is not viscous flow but plastic flow and the plastic flow resistance conflicts with the viscous flow resistance at the preferred condition for Si particle refinement. On the basis of these temperature dependences, the power-law model of Equation (9) was derived to evaluate the effect of viscoplastic flow dominated by plastic flow on the refinement of Si particles, which led to Equation

(11).

Unlike the relationship between shear rate and Si particle size shown in Figure 10, Si particle size as a function of the equivalent strain or the mean strain rate varies widely, as shown in Figures 5 and 6, respectively. Similar tendencies are evident in Figures 8 and 9, which show the Si particle size as a function of power and power rate, respectively. Thus, the relationship between particle size and equivalent strain, mean strain rate, power, or power rate cannot be expressed by a concise formula such as that in Equation (9). In the case of these parameters, great variability arises from the fact that the effects of deformation, *i.e.*, a decrease in height, on each value are relatively small: the effects in obvious cases are only approximately proportional to $v/\Delta h$ in Equations (2) and (4). In contrast, the effect of deformation on the shear rate is more obvious and the shear rate is proportional to $v/h^{2.5}$ in Equation (6), which gives a greater normalized range on the abscissa axis. The dependence on the shear rate causes the experimental results to follow the unique empirical equation as represented in Figure 10. In discussing the causes of the results obtained in these experiments, we note that parameters such as the equivalent strain, mean strain rate, power, and power rate are not the predominant factor governing Si particle refinement. These parameters mutually affect each other, and these mutual effects apparently lead to the eventual refinement of the Si particles.

The power-law model of Equation (11) was derived from the aforementioned viewpoint. If the test temperature approaches T_m = 850 K (577 °C), the power-law index and constant converged to −∞ and 0 mm, respectively; the semisolid forming gradually returns to a plastic forming, and the refinement of Si particles is accelerated. In contrast, if the test temperature is increased, the effect of Si particles refinement is lost because the power-law index and constant approach 0 and 0.27 mm (the size of the as-received particles), respectively; *i.e.,* the process transitions to a casting and loses the effect of Si particles refinement. If the factor governing the viscoplastic flow is changed to viscous flow with increase in working temperature, Equation (11) may no longer be valid, as noted in the discussion of Figures 2 and 3. Thus, the effects of temperature difference and shear rates on the Si particle refinement were successfully evaluated. We conclude that achieving refinement of Si particles requires high-speed operation at a temperature just above the melting point of 850 K (577 °C), which must be the optimum near-net forming condition, where the plastic flow dominates the viscoplastic flow and interacts with viscous flow. Further experiments are required to verify this hypothesis.

IV. SUMMARY

Experiments to investigate the possibility of refining the coarse Si particles in a hypereutectic Al–25 mass% Si alloy to enable its use in practical application were conducted using uniaxial compression tests at temperatures over the eutectic melting point T_m = 850 K (577 °C). The test conditions comprised a combination of temperatures T = 853 K (580 °C) and 863 K (590 °C), compression rates v = 5, 25, and 125 mm/min, and compression strokes Δh = 5, 10, and 12 mm with cylindrical specimen 15mm in height. The following conclusions were drawn on the basis of this work:

1. The deformed specimens exhibited the barrel shaped features without exception, unlike the results obtained in drop forge experiments. The use of a very slow compression rate must have constrained the movement of the liquid component of the semi-solid specimens. The results of the experiments suggested that the dominant factor governing the viscoplastic flow under the experimental conditions is the plastic flow.

2. Si particles became granular and more refined under test conditions of the lower test temperature, the highest compression rate, and the longest compression stroke. Finest Si particles were obtained under test conditions of T = 853 K (580 °C), a compression stroke of Δh = 12 mm, and a compression rate of v = 125 mm/min, and the particle size was refined from 0.27 mm in the as-received sample to 0.12 mm in the refined sample.

3. Parameters such as the equivalent strain, mean strain rate, power, and power rate were not the predominant factor governing Si particle refinement; therefore, the Si particle size could not be expressed by a concise formula as a function of such parameters. These parameters apparently interacted with one another, and these mutual effects appeared to lead to the eventual refinement of the Si particles.

4. The particle size decreased with increasing shear rate, and the effect of the shear rate, $\dot{\gamma}$[s^{-1}], and the test temperature, T [K], on the Si particle size, G [mm], were expressed using an empirical power-law equation: $G = 0.08(T - T_m)^{0.4}\dot{\gamma}^{-0.24/(T-T_m)}$ This relation indicated that high shear rate operation at a temperature just above the melting point must be the optimum conditions for refining the Si particles.

REFERENCES

[1] B.K. Prasad, K. Venkateswarlu, O.P. Modi, A.K. Jha, S. Das, R. Dasgupta, and A.H. Yegneswaran, "Sliding wear behavior of some Al–Si alloys: Role of shape and size of Si particles and test conditions", Metall. Mater. Trans. A, Vol. 29A, No. 11 , pp. 2747-2752, 1998.

[2] J.U. Ejiofor and R.G. Reddy, "Developments in the processing and properties of particulate Al–Si

composites", JOM, Vol. 49, No. 11, pp. 31-37, 1997.

[3] A. Hekmat-Ardakan and F. Ajersch, "Thermodynamic evaluation of hypereutectic Al–Si (A390) alloy with addition of Mg", Acta Mater., vol. 58, pp. 3422-3428, 2010.

[4] A. Mazahery and M.O. Shabani, "Modification mechanism and microstructural characteristics of eutectic Si in casting Al–Si alloys: A review on experimental and nuemerical studies", JOM, vol.66, No.5, pp. 726-738, 2014.

[5] Y. Fukui, "Fundamental investigation of functionally gradient material manufacturing system using centrifugal force", JSME Int. J Series III, Vol. 34, No. 1, pp. 144-148, 1991.

[6] Y. Watanabe, N. Yamanaka, and Y. Fukui, "Control of composition gradient in a metal-ceramic functionally graded material manufactured by the centrifugal method", Composites Part A, Vol. 29A, Nos. 5,6, pp. 595-601, 1998.

[7] Y. Fukui, H. Okada, N. Kumazawa, and Y. Watanabe, "Near net shape forming of Al–Al$_3$Ni FGM over eutectic melting temperature", Metallurgical and Materials Transactions A, Vol. 31A, No. 10, pp. 2627-2636, 2000.

[8] K. Yamagiwa, Y. Watanabe, K. Matsuda, Y. Fukui, and P. Kapranos, "Characteristic of Al–Al$_3$Fe eco-functionally graded material through near-net-shape forming over eutectic melting temperature", Materials Science and Engineering A, Vol. A416, Nos. 1-2, pp. 80-91, 2006.

[9] D. Nara, N. Kumazawa, and Y. Fukui, "Semi-solid forming of Al–Si functionally graded material and refinement of Si particles", Transactions of the JSME, Series A, Vol. 78, No.795, pp.1575-1582, 2012 (in Japanese).

[10] M.C. Flemings, "Behavior of metal alloys in the semisolid state", Metallurgical Transactions A, Vol. 22A, No.5, pp. 957-981, 1991.

[11] D.H. Kirkwood, M. Suéry, P. Kapranos, H.V. Atkinson, and K.P. Young, "Semi-solid Processing of Alloys", Springer Berlin Heidelberg, Germany, 2010.

[12] D.S.B. Heidary and F. Akhlaghi, "Experimental Investigation on the reological behavior of hypereutectic Al–Si alloys by a precise rotational viscometer", Metall. Mater. Trans. A, vol. 41A, No. 12, pp. 3435-3442, 2010.

[13] H.M. Guo, L.J. Wang, Q. Wang, and X.J. Yang, "Effect of solid-liquid mixing on microstructur of semi-solid A356 aluminum alloy", Metall. Mater. Trans. B, vol. 45B, No. 8, pp. 1490-1495, 2014.

[14] T. B. Massalski, ed., "Binary Alloy Phase Diagrams, Second Edition Plus Updates on CD-ROM Version 1.0", *ASM International*, 1996.

[15] D. Nara, N. Kumazawa, and Y. Fukui, Deformation behavior of semi-solid hypereutectic Al–Si alloy compressed in the drop-forge viscometer, Transactions of the JSME (in Japanese), Vol. 80, No.812, [DOI: 10.1299/transjsme.2014smm0081], 2014.

[16] R. Papirno, "Axial Compression Testing", Metals Handbook Ninth Edition, Vol.8 Mechanical Testing, American Society for Metals, pp.55-58, 1985.

[17] E.W. Hart, "Theory of the tensile test", *Acta Metallurgica,* Vol.15, No.2, pp. 351-355, 1967.

[18] J.A. Yurko and M.C. Flemings, "Rheology and microstructure of semi-solid aluminum alloys compressed in the drop forge viscometer", Metallurgical and Materials Transactions A, Vol. 33A, No.8, pp. 2737-2746, 2002.

[19] V. Laxmanan and M.C. Flemings, "Deformation of semi-solid Sn–15 pct Pb alloy", Metallurgical Transactions A, Vol. 11A, No.12, pp.1927-1937, 1980.

[20] D. Kececioglu and J.A. Jacks, "The Arrhenius, Eyling, inverse power-law and combination models in accelerated life testing", Reliability Engineering, Vol. 8, pp.1-9, 1984.